Surfaces and Interfaces 29 (2022) 101720

Contents lists available at ScienceDirect

Surfaces and Interfaces

journal homepage: www.sciencedirect.com/journal/surfaces-and-interfaces

Mechanochemical route for tetra amino zinc phthalocyanine embedded PANI sensitized Fe_2O_3 heteroarchitecture for photodegradation of dyes under the influence of low power LED light source

Shwetha Rajappa [a], Poornima Gubbi Shivarathri [a], Malayanur Laxmipathi Aruna Kumari [b], Divyashree Kalenahally Swamygowda [c], Mruthyunjayachari Chattanahalli Devendrachari [d], Harish Makri Nimbegondi Kotresh [a,*]

[a] Department of Chemistry, Acharya Institute of Technology, Bangalore, 560107
[b] Department of Chemistry, The Oxford College of Science, Bengaluru, 560102
[c] Department of Soil Science and Agricultural Chemistry, College of Agriculture, VC Farm, Mandya, 571402
[d] Department of Chemistry, Indian Institute of Science, Education, and Research, Pune, 411008

ARTICLE INFO

Keywords:
Mechanochemical route
phthalocyanine
Hybrid photocatalyst
photodegradation
LED light source

ABSTRACT

In the present work, we demonstrate a facile, simple and effective solvent-free rapid mechanochemical approach for the synthesis of tetra amino zinc phthalocyanine engrained PANI sensitized Fe_2O_3 hybrid (TAZnPc-PANI@Fe_2O_3) photocatalyst. Fourier transform infrared spectroscopy (FTIR), powder X-ray diffraction (XRD) and scanning electron microscopy (SEM), Solid state diffuse reflectance spectrophotometer have been used to characterize the structure, size, morphology and optical properties of TAZnPc-PANI@Fe_2O_3 photocatalyst. Cationic methylene blue (MB) and anionic Eosin Y (EY) dyes were chosen as modular pollutants to investigate photodegradation competence of Fe_2O_3 alone and TAZnPc-PANI@Fe_2O_3 hybrid photocatalyst under the influence of the low power white LED (16 W) as visible light source. Influence of operational parameters such as catalyst loading, contact time, pH of the medium and reusability of the catalyst on the dye degradation are investigated. The obtained results established that photosensitization of Fe_2O_3 with tetra amino zinc phthalocyanine embedded PANI (TAZnPc-PANI) significantly enhanced the photocatalytic performance towards photodegradation of MB and EY dyes. The photodegradation of MB and EY under optimised conditions was found to be ~95 % in 80 min.

1. Introduction

In the past few decades, with increased population and industrialization the availability of clean water for both domestic and industrial applications have become a global concern [1,2]. Wastewater from the textile, paper and other industries rich with toxic and non-biodegradable coloring matter when discharged into the natural water bodies seriously threatens the whole ecosystem [3,4]. The dyes released from textile industries are highly toxic and carcinogenic in nature, so causes serious environmental problems including human health and aquatic medium [5, 6]. From the viewpoint of the environment issues, wastewater treatment and recycling can be considered as one of the most important challenges in recent years. It should be noted that admirable developments have been made to convert hazardous toxic pollutants to less toxic or nontoxic material by photocatalytic degradation of toxic organic materials by means of photoactive materials [7-10] and by using micro-organisms [11]. Reports advocate that compared to pristine semiconductor metal oxides, photosensitization of metal oxides with various photo sensitizers and carbon-based materials can significantly enhance the photocatalytic activity of the photocatalysts in the presence of the light. [12-18]

During the past decade the advanced properties of metal phthalocyanines (MPc's), polyaniline (PANI) and other conjugated nitrogen rich heterogeneous hybrid systems has been explored as organic functional materials in numerous emerging technologies, including energy conservation and storage, molecular electronics, sensors and hydrogen fuel production [19-27]. Materials with an extended π-conjugated electron system poses excellent stability, improved conductivity, exceptional

* Corresponding author
E-mail address: mnkharish11@gmail.com (H.M.N. Kotresh).

https://doi.org/10.1016/j.surfin.2022.101720
Received 2 October 2021; Received in revised form 29 December 2021; Accepted 1 January 2022
Available online 4 January 2022
2468-0230/© 2022 Elsevier B.V. All rights reserved.

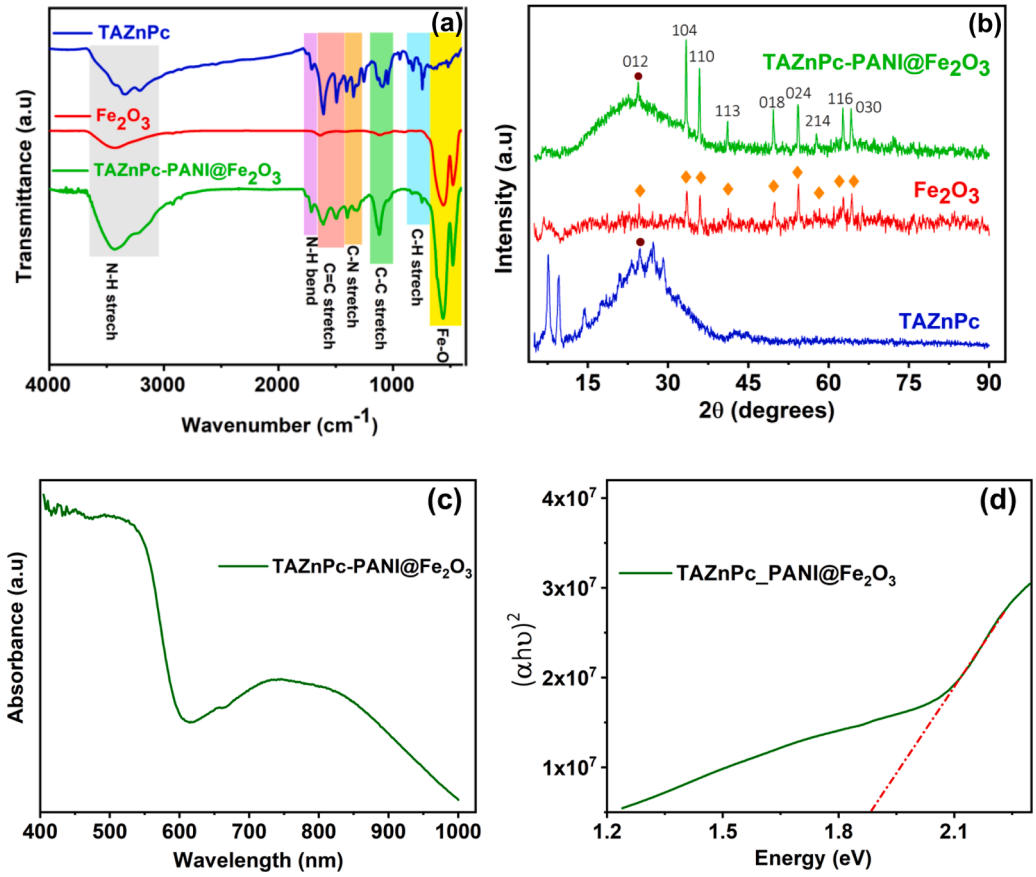

Fig. 1. a) FTIR spectra of Fe_2O_3, TAZnPc and TAZnPc-PANI@Fe_2O_3, b) X-ray diffraction study of Fe_2O_3, TAZnPc and TAZnPc-PANI@Fe_2O_3, c) Solid state diffuse reflectance spectra of TAZnPc-PANI@Fe_2O_3, d) Band gap estimation of TAZnPc-PANI@Fe_2O_3.

electrochemical performance, biomedical applications, photcatalytic activity [28-33]. In this context the MPc's, substituted MPc's and PANI sensitized semiconductor metal oxides have gained immense attention in recent years in many technological applications including photocatalyst for environmental remediation for their outstanding stability and fascinating optical property as they can absorb in the longer wavelength section of the visible light solar spectrum [34-41].

Mechanochemistry is a branch of solid-state chemistry which investigates effect of mechanical energy in variety of organic and inorganic transformations mainly under solvent free or solvent deficient conditions [42-46]. Over the past decades, mechanochemistry has blossomed briskly due to its simplicity, high conversion and yields, often-short reaction time, easy operational procedure and reduced pollution [47]. Divers organic and inorganic transformations has been realized via mechanochemistry [48-51]. Further organic-inorganic hybrid materials acquired through mechanochemistry have become one of the most intensely researched areas of materials chemistry [52-54].

Traditionally high-power mercury, halogen and tungsten lamps involving hazardous components, are used as visible light source in photocatalytic studies [55-58]. However, these light sources have some serious issues such as use of environmental hazardous elements, heating effect, shorter lifetime and they require higher energy to operate. Additionally excessive heating effect of the light source requires additional component to bring down the reactor temperature to run in comfort. Recently energy efficient, low power LED as light source for photocatalytic studies have been documented with significant photocatalytic competence [59-65]. Although low powered LED have many advantages, very less work has been done on the utilization of low power LEDs for photo degradation studies.

In this study, to stimulate the photocatalytic efficiency of the Fe_2O_3, TAZnPc engrained PANI sensitized Fe_2O_3 hybrid photocatalyst was successfully fabricated via a simple mechanochemical route. Cationic methylene blue (MB) and anionic Eosin Y (EY) dye was chosen as modular pollutants to evaluate the effect of photosensitization of Fe_2O_3 nanoparticles with TAZnPc engrained PANI under the influence of the low power white light LED (16 W) as visible light source.

2. Experimental section

2.1. Materials and methods

Reagents such as 4-nitrophthalophthalimide, ammonium heptamolybdate tetrahydrate, sodium sulfide nonhydrate and aniline were purchased from Sigma Aldrich. Other chemicals were obtained from Merck (India). Before use, aniline was distilled and stored in the dark. Double distilled water was used to prepare stock and feed solutions.

2.2. Preparation of Ferric oxide Fe_2O_3 nano particles

Ferric oxide nanoparticles were synthesized by adopting previously reported procedure [66]. In brief, 5 g of $FeCl_3.6H_2O$ was dissolved in 1 L of double distilled water followed by the addition of 10 % of aqueous NH_3 solution to the above solution until the pH condition changes to 2-3. A dark brown coloured metal hydroxide precipitate is formed and this precipitate is allowed to age in the solution for five days at ambient conditions. Excess double distilled water was added to the above suspension and stirred vigorously for 3 h. The precipitate was first washed thoroughly with dilute NH_3 solution and later with double distilled water until all the chloride ions were removed. The solid thus obtained

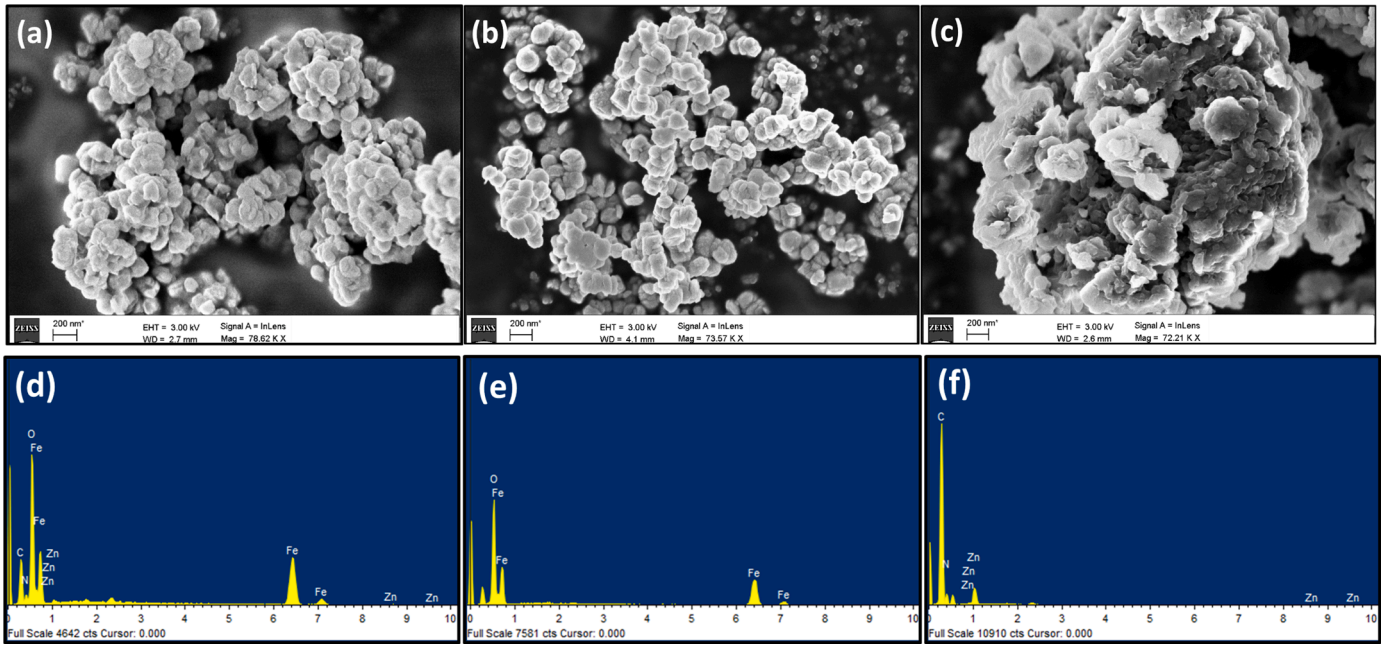

Fig. 2. (a-c) FESEM images of TAZnPC-PANI@Fe_2O_3, Fe_2O_3 and TAZnPc. (d-f) Energy-dispersive X-ray spectrum (EDX) of TAZnPC-PANI@Fe_2O_3, Fe_2O_3 and TAZnPc

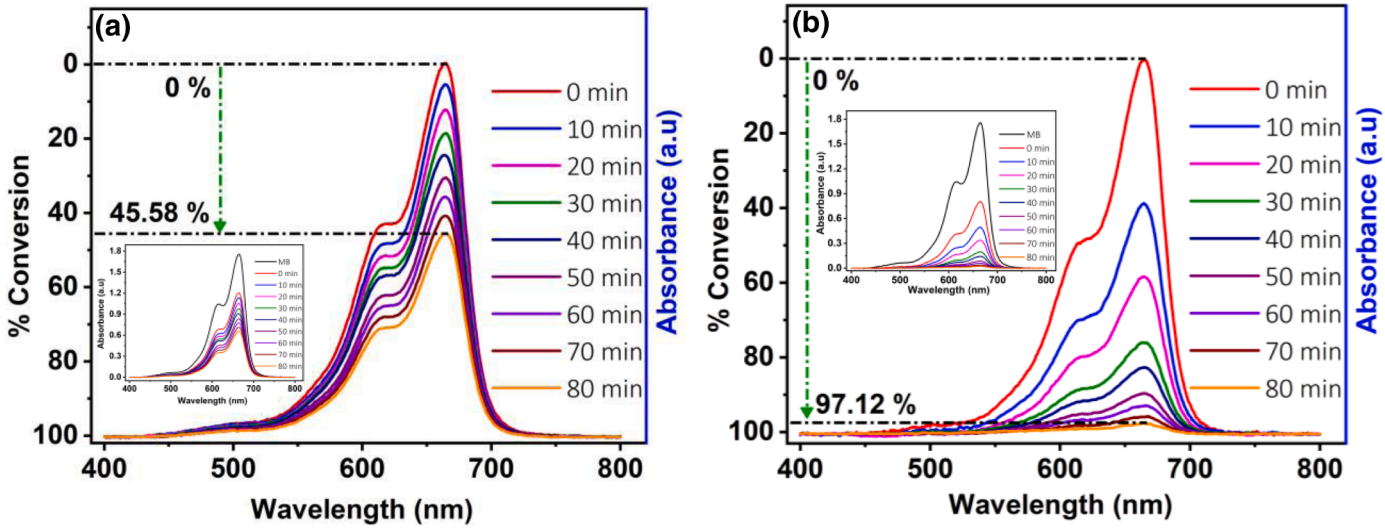

Fig. 3. UV–vis absorption spectra of MB photo degradation in the presence of (a) Fe_2O_3 and (b) TAZnPc-PANI@Fe_2O_3 hybrid catalyst under identical conditions.

was then dried in an oven at 100 °C followed by calcination at 400 ℃ for 4 h to get crystalline Fe_2O_3 sample.

2.3. Synthesis of β-Tetra amino zinc phthalocyanine

Tetra amino zinc phthalocyanine was synthesized by adopting previously well documented procedure [21]. In brief, by using 4-Nitro phthalimide as raw material we have synthesized β-tetra nitro phthalocyanine. Followed by the reduction of β-tetra nitro phthalocyanine using $Na_2S.9H_2O$ to get β-tetra amino zinc phthalocyanine (β- TAZnPc). The resultant product was washed with hot HCl aqueous solution and NaOH aqueous solution in turn for several times. Subsequently, the solid was centrifuged with distilled water followed by alcohol wash several times.

2.4. Preparation of TAZnPc-PANI@Fe_2O_3 and PANI@Fe_2O_3 hybrid photocatalyst

Fe_2O_3 nanoparticles (100 mg) and tetra amino zinc phthalocyanine (20 mg) were pulverized with 20 mg aniline for 5 minutes in agate mortar and pestle followed by the addition of ammonium per sulphate. The reaction mixture was thoroughly mixed for additional 15 minutes. Then the reaction mixture was incubated for 1 hour at room temperature. The product TAZnPc-PANI@Fe_2O_3 obtained was thoroughly washed with water followed by ethanol and dried in oven at 100 °C for 5 h. Scheme 1 represents the schematic diagram for mechanochemical synthesis of TAZnPc-PANI@Fe_2O_3. PANI@Fe_2O_3 was synthesized adopting the above mentioned procedure in the absence of TAZnPc.

3. Photocatalysis experiments

The photocatalytic performance of the synthesized nanomaterials

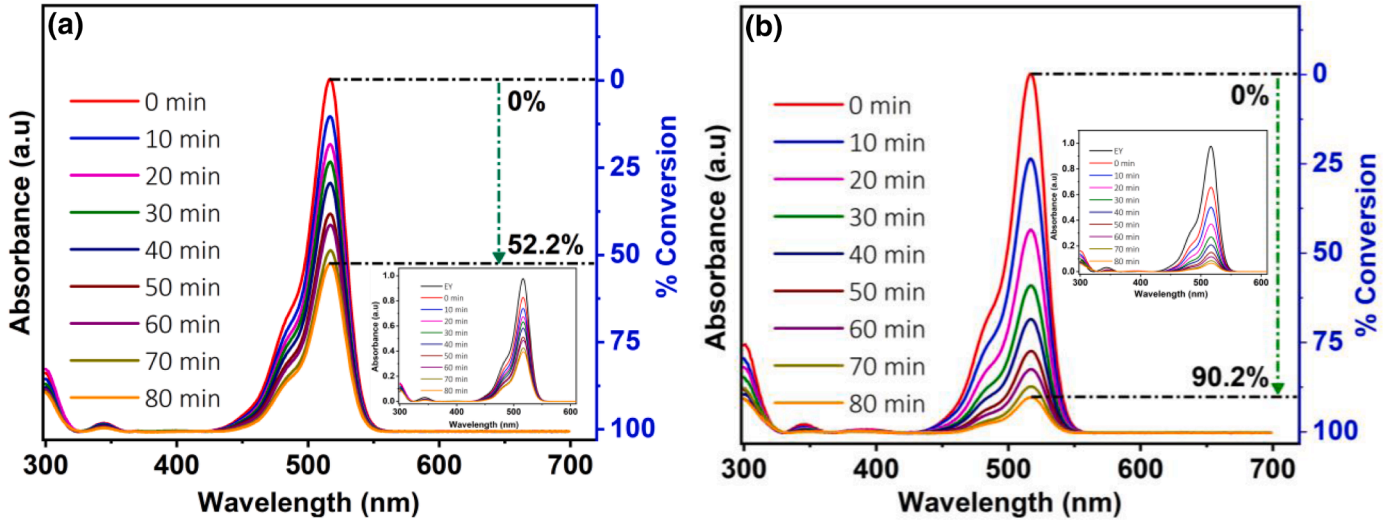

Fig. 4. UV–vis absorption spectra of EY photo degradation in the presence of (a) Fe_2O_3 and (b) TAZnPc-PANI@Fe_2O_3 hybrid catalyst under identical conditions.

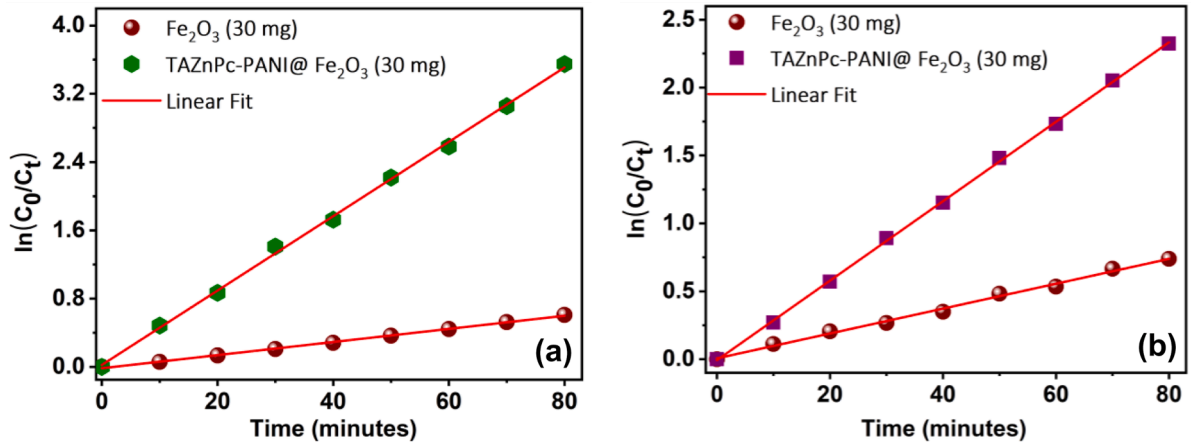

Fig. 5. Kinetic study: Plot of ln $\frac{C_0}{C_t}$ as a function of light irradiation time for Fe_2O_3 and TAZnPc-PANI@Fe_2O_3 hybrid catalyst (a) MB and (b) EY

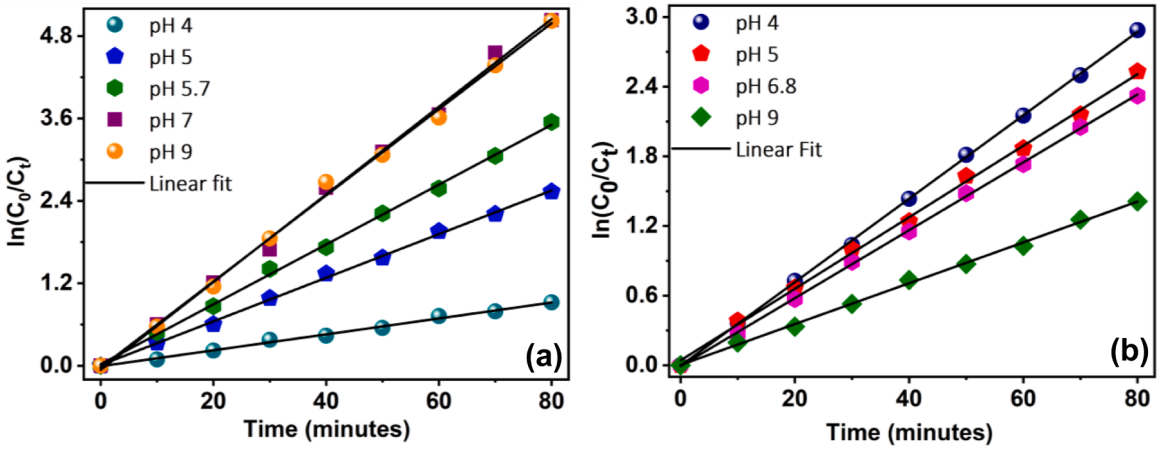

Fig. 6. Kinetic study: Plot of ln $\frac{C_0}{C_t}$ as a function of light irradiation time at different pH for TAZnPc-PANI@Fe_2O_3 hybrid catalyst (a) MB and (b) EY

was evaluated for the photocatalytic degradation of cationic MB and anionic EY dye in aqueous solution under the influence of low power LED light source. Solutions of dyes were prepared by dissolving the MB and EY in double distilled water to obtain a solution of 10 ppm concentration. The photocatalytic degradation experiments, was carried out in a photoreactor provided with a magnetic stirrer and 16 W low power LED visible light source. In a typical process, known amount of photocatalyst was suspended in 100 mL model dye solution. Before irradiation, the dye solution along with the photocatalyst was stirred in the dark for 30 min to achieve adsorption-desorption equilibrium. The

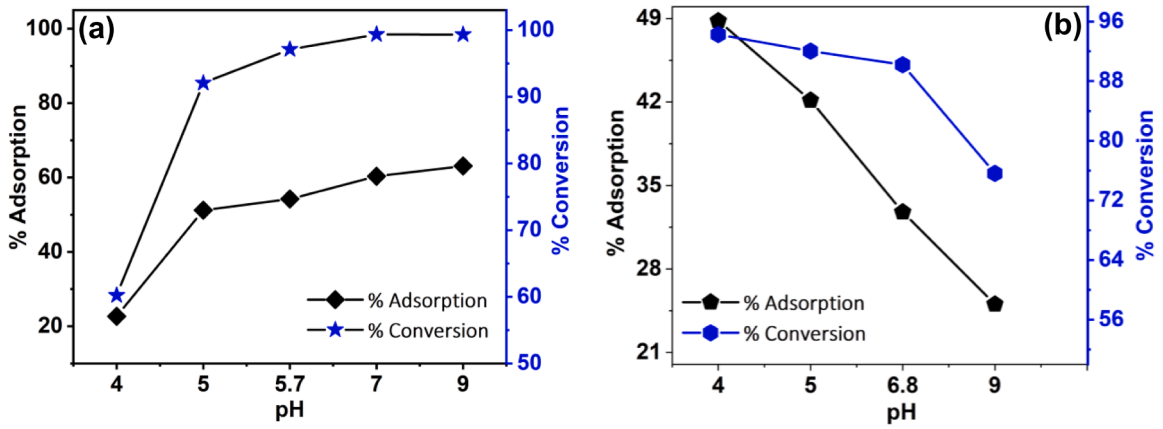

Fig. 7. Effect of pH on % adsorption and % conversion of dye in the presence of 30 mg TAZnPc-PANI@Fe_2O_3 (a) MB and (b) EY

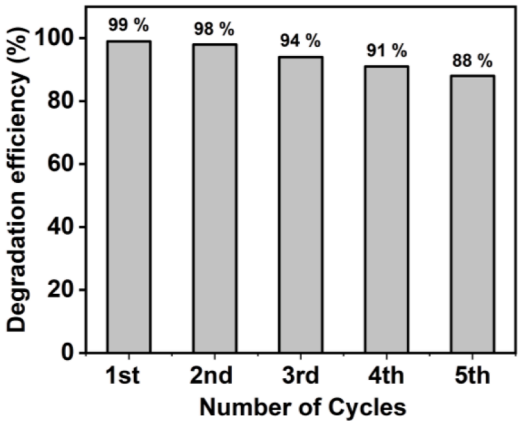

Fig. 8. Reusability assessment of the TAZnPc-PANI@Fe_2O_3 towards photocatalytic degradation of MB at pH 7

photocatalytic degradation process was monitored by recording the characteristic absorption for MB and EY respectively by UV–vis spectrophotometer. The % degradation of the dye was determined by using the following relation

$$\%\text{Degradation} = \frac{C_O - C_t}{C_O} \times 100$$

Where C_O is the concentration of dye at 0^{th} time and C_t the concentration of dye at t minutes. The influence of operational parameters such as photocatalyst loading, effect of contact time and impact of pH on photocatalytic degradation of MB and EY was investigated.

4. Results and discussion

4.1. FTIR Analysis

The FTIR spectra of α-Fe_2O_3, TAZnPc and TAZnPc-PANI@Fe_2O_3 are shown in Fig. 1a and were recorded in the range of 400-4000 cm^{-1}. The FTIR spectrum of Fe_2O_3 exhibited characteristic metal-oxygen bond formation in the region of 400-700 cm^{-1}. The absorption band at 473 cm^{-1} correspond to the stretching vibration of Fe–O and the band at 564 cm^{-1} is associated with Fe-O-H stretching vibration. The bands at 3434 cm^{-1} and 1639 cm^{-1} arise due to O–H stretching vibration of surface-adsorbed water molecules on Fe_2O_3 [67].

The FTIR spectrum of TAZnPc shows characteristic broad absorption bands at 3340 and 3210 cm-1 for γ N-H and δ N-H stretching vibrations and intense peak at 1607 cm-1 for -N-H in-plane bending vibrations. The bands at 1347, 1092, 1047, 827, 744 cm^{-1} are assignable to the skeleton stretching of TAZnPc. A very weak signal observed for the TAZnPc at 2923 cm^{-1} is due to C–H stretching vibration on the periphery of the phthalocyanine moiety. Signals observed in the range of 1496 cm^{-1} peaks was assigned to C=C aromatic stretching frequency [68]. The peaks found in TAZnPc can be observed in TAZnPc-PANI@Fe_2O_3, but are absent in Fe_2O_3. The disappearance of primary N–H stretching bands at 3340 and 3210 cm^{-1} in TAZnPc-PANI@Fe_2O_3 indicates the involvement of TAZnPc in polymerization. In addition, presence of absorption bands at 477 cm^{-1} and 563 cm^{-1} in TAZnPc-PANI@Fe_2O_3 corresponding to Fe–O and Fe-O-H stretching vibration indicated the successful functionalization of TAZnPc-PANI on Fe_2O_3 nanoparticles.

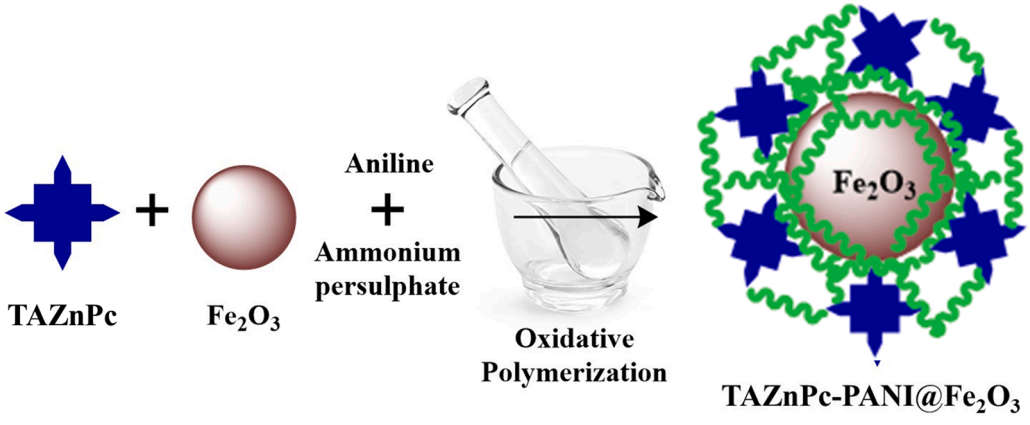

Scheme 1. Schematic representation for mechanochemical synthesis of TAZnPc-PANI@Fe_2O_3

4.2. X-ray diffraction (XRD) analysis

The XRD patterns of the synthesized TAZnPc-PANI@Fe_2O_3, Fe_2O_3, and TAZnPc are shown in Fig. 1b. The diffraction peaks of the TAZnPc at $2\theta = 25.51^\circ$ were broad and weak, suggests amorphous nature of phthalocyanine (JCPDS Card No: 39-1882) [69-71]. In case of Fe_2O_3 the diffraction peaks observed at $2\theta = 24.70^\circ$, 33.35°, 35.80°, 41.17°, 49.62°, 54.35°, 57.82°, 62.58° and 64.13° attributed to the (012), (104), (110), (113), (024), (116), (214) and (300) crystal planes of nano-structured α-Fe_2O_3 phase (JCPDS Card No: 08-1248) [72-74]. While in the XRD spectrum of TAZnPc-PANI@Fe_2O_3 the peaks corresponding to the TAZnPc are perceived as a broad peak at $2\theta = 24.04^\circ$ with slight down shift in 2θ value, along with all the corresponding peaks of Fe_2O_3. Here the high crystallinity of Fe_2O_3 masked the diffraction peaks of TAZnPc-PANI. So, the presence of TAZnPc-PANI is observed as a broad peak with slight down shift in 2θ value in the TAZnPc-PANI@Fe_2O_3 and this clearly confirms the formation of homogeneous composite TAZnPc-PANI@Fe_2O_3. The crystal grain size for the synthesised TAZnPc, Fe_2O_3, and TAZnPc-PANI@Fe_2O_3 were calculated using Scherrer equation. The full width at half maximum of the characteristic peak for the TAZnPc, Fe_2O_3, and TAZnPc-PANI@Fe_2O_3 resulted 0.62 nm, 15.75 nm, and 30.65 nm respectively.

4.3. Solid state diffuse reflectance spectra

The optical properties of Fe_2O_3, PANI@Fe_2O_3 and TAZnPc-PANI@Fe_2O_3 were analysed in Solid state diffuse reflectance spectrometry in the spectral range, from 400 to 1000 nm. The diffuse reflectance spectra of TAZnPc-PANI@Fe_2O_3 presented in Fig. 1c. shows broad absorption in visible region (600-990 nm) with a small hump at 653 nm. The Fig. 1d. represents the graph of $(\alpha h\nu)^2$ versus $h\nu$ (eV) and the estimated band gap for TAZnPc-PANI@Fe_2O_3 was found to be 1.88 eV. The absorption spectrum of Fe_2O_3 and PANI@Fe_2O_3 presented in Fig Sl (a) and (b) exhibited a peak at around 800 and 850 nm respectively. In additional sluggish peak at ~ 650 nm was observed when Fe_2O_3 is functionalized with PANI. The estimated band gap was found to be in the order Fe_2O_3 (1.979 eV) > PANI@Fe_2O_3 (1.975 eV) > TAZnPc-PANI@Fe_2O_3 (1.88 eV).

4.4. FESEM and EDX analysis

The morphology of the synthesized compound and their composites were characterized using FESEM analysis. Fig. 2. (a-c) shows the FESEM images of TAZnPC-PANI@Fe_2O_3, Fe_2O_3, and TAZnPc. The synthesized Fe_2O_3 nanoparticles exhibited distorted spherical shaped particles with agglomeration, with an average diameter of about 100 nm. The observed agglomeration in Fe_2O_3 nanoparticles can be attributed to the absence of surfactants during the synthesis. In case of TAZnPC-PANI@Fe_2O_3 the morphology was quite similar to Fe_2O_3, but with increased agglomeration due to surface functionalization of TAZnPC-PANI on Fe_2O_3 nanoparticles. The morphology of TAZnPc showed clustered flakes with a non-uniform shape and size distribution.

EDX analysis further supported the above interpretations. Fig. 2. (d-f) confirmations the existence of Fe and O in Fe_2O_3 nanoparticles, whereas the existence of Zn, C and N along with Fe and O in TAZnPC-PANI@Fe_2O_3 hybrid nanocomposite provides the evidence for the surface functionalization of TAZnPC-PANI on Fe_2O_3 nanoparticles. The elemental fraction of the elements in Fe_2O_3 nanoparticle was found to be Fe (29.53%) and O (70.47%) whereas in TAZnPC-PANI@ Fe_2O_3 nanocomposite the elemental fraction was observed to be; C (30.58%), N (7.75%), O (46.02%) Zn (0.33%) and Fe (15.32%).

4.5. Photocatalytic activity

Under the influence of low power LED light source, the photocatalytic activity of Fe_2O_3, PANI@Fe_2O_3 and TAZnPc-PANI@Fe_2O_3 was investigated for the photo degradation of cationic MB and anionic EY dye in aqueous solution. Preliminary investigation to assess the photocatalytic efficacy of Fe_2O_3 and TAZnPc-PANI@Fe_2O_3 was undertaken under natural pH for 10 ppm dye solutions. Fig. 3 (a-b) shows UV–vis absorption of MB photo degradation in the presence of Fe_2O_3 and TAZnPc-PANI@Fe_2O_3 hybrid catalyst under identical conditions. It was found that TAZnPc-PANI@Fe_2O_3 hybrid exhibits superior photocatalytic activity ~97 % compared to pure Fe_2O_3 ~46% towards MB photo degradation. Fig. 4 (a-b) shows UV–vis absorption of EY photo degradation in the presence of Fe_2O_3 and TAZnPc-PANI@Fe_2O_3 hybrid catalyst under identical conditions. It was confirmed that the TAZnPc-PANI@Fe_2O_3 hybrid exhibits superior photocatalytic activity ~90% compared to pristine Fe_2O_3 ~52 % towards EY photo degradation. In the presence of TAZnPc-PANI@Fe_2O_3 hybrid catalyst efficient degradation has been accomplished, resulting in the > 90% degradation for both MB and EY dyes in 80 min, while Fe_2O_3 demonstrated <55% of MB and EY dye degraded under natural pH. Fig. S6 (a-b) shows UV–vis absorption of MB and EY photo degradation in the presence of PANI@Fe_2O_3 hybrid catalyst under identical conditions. No significant changes in photo degradation efficacy were observed in PANI@Fe_2O_3 as compared with pristine Fe_2O_3.

The rate constant for the dye photo-degradation catalyzed by Fe_2O_3 and TAZnPc-PANI@Fe_2O_3 were evaluated by taking the slope from the plot of $\ln \frac{C_0}{C_t}$ vs light irradiation time. Fig. 5 (a-b) shows nearly a linear relationship between $\ln \frac{C_0}{C_t}$ and light irradiation time t indicating that the photo degradation reaction of MB and EY dyes follows first-order reaction kinetics model. The reaction rate constant k was calculated from the slope of the plot of $\ln \frac{C_0}{C_t}$ against light irradiation time t. The rate constant for the MB dye degradation on Fe_2O_3 and TAZnPc-PANI@Fe_2O_3 was found to be 0.0076 and 0.0436 min^{-1} whereas the rate constant for the EY dye degradation on Fe_2O_3 and TAZnPc-PANI@Fe_2O_3 was found to be 0.0092 and 0.029 min^{-1} respectively [Table S1]. The obtained results unambiguously proves that the photodegradation efficiency of TAZnPc-PANI@Fe_2O_3 for MB and EY dye occurs at a faster rate and is almost 6 times as high as Fe_2O_3 for MB and 3 times as high as Fe_2O_3 for EY. From these results, it is well stated that enhancement of photo-degradation efficiency and subsequent rate constants were realized for TAZnPc-PANI@Fe_2O_3, demonstrating it as a potential photocatalyst for mineralization and oxidation of organic pollutants.

The exceptional photocatalytic activity of TAZnPc-PANI@Fe_2O_3 hybrid compound can be attributed to the strong coupling between TAZnPc, PANI and Fe_2O_3, which facilitates the effective interfacial charge transfer. The TAZnPc entrapped PANI@Fe_2O_3 hybrid photocatalyst under the influence of visible light irradiation, absorb the light energy and electrons get excited from the HOMO to the LUMO state. This results in the generation of superoxide radicals $O_2^{\bullet}$ and hydroxyl radicals $HO^{\bullet}$ by transfer of excited electron from TAZnPc entrapped PANI to the conduction band of Fe_2O_3. Thus, TAZnPc entangled PANI acts as a mediator for transferring electrons from the sensitizer to substrate electron acceptor Fe_2O_3, resulting in effective photo degradation of MB and EY dyes.

4.5.1. Influence of catalyst loading on the dye degradation

Catalyst loading is one of the key factors that can significantly influence the photocatalytic degradation. Initially in order to understand the optimum loading of photocatalyst for effective dye removal, the influence of photocatalyst loading on the photodegradation of MB was explored. Fig. S2 shows the effect of catalyst loading of 10, 20, 30 and 40 mg of TAZnPc-PANI@Fe_2O_3 hybrid on the photo degradation of MB under natural pH. It can be observed that photocatalytic efficacy increased with the increase in catalyst loading, indicating the availability of active sites on the photocatalyst surface for the adsorption of dyes. When the catalyst loading was 30 mg, the degradation efficiency was > 95% for MB in 80 min. No considerable change in degradation efficiency was observed for 40 mg of catalyst loading. Hence, the

optimal dosage of photocatalyst loading for photodegradation was determined as 30 mg.

4.5.2. Influence of the pH

The zero-point charge (ZPC) is surface charge characteristics of the nanoparticles which depends on the pH of the solution, and can influence the percentage adsorption characteristics of dye molecules on surface of photocatalyst. In the degradation process first step involves the adsorption of dye molecule on photocatalyst and this step depends on the ZPC of the photocatalyst. The ZPC of TAZnPc-PANI@Fe_2O_3 was found to be 4.4, this indicates that surface of TAZnPc-PANI@$Fe2O_3$ is positively charged at pH value lower than 4.4 and negatively charged at pH greater than 4.4 shown in Fig. S3. Therefore, effect of pH on dye degradation process was studied at different pH values ranging from 4 to 9. The pH of the dye solution for photocatalytic experiments was adjusted by addition of either NaOH or HCl solution.

The pH dependent photodegradation of MB are presented in Figure 6a and it was observed that photodegradation of MB increases with increase in pH. At pH 4.0, 5.0, 5.7, 7.0 and 9.0 the percentage removal was found to be 60, 92, 97, 99 and 99 % respectively in 80 min under visible light irradiation. UV–vis absorption and % conversion of MB in the presence of TAZnPc-PANI@Fe_2O_3 at pH 4.0, 5.0, 7.0 and 9.0 respectively are presented in Fig. S4 (a-d).

Kinetic study portrays that degradation follows pseudo first order kinetics [Fig. 6a]. The observed slope was found to be 0.0116, 0.0318, 0.0436, 0.0639 and 0.0627 min^{-1} respectively for pH 4.0, 5.0, 5.7, 7.0 and 9.0. As expected at lower pH, the dye degradation was moderately less and at high pH the dye degradation is significantly enhanced. This can be attributed to the fact that at higher pH, the surface of photocatalyst is more negatively charged, and MB dye is a cationic dye that favours the efficient adsorption of MB dye on photocatalyst. Optimum degradation of MB dye is obtained at pH 7 where in 99 % degradation was achieved in 80 min under visible light irradiation.

Further degradation of EY dye was found to increases with decrease in pH. At pH 4.0, 5, 6.8 and 9.0 the percentage removal was found to be 94.4, 92, 90 and 75% respectively in 80 min under visible light irradiation. Kinetic study portrays that degradation follows pseudo first order kinetics [Fig. 6b]. The observed slope was found to be 0.0359, 0.0308, 0.0292 and 0.0175 min^{-1} respectively for pH 4.0, 5, 6.8, and 9.0 respectively. At lower pH, the dye degradation got significantly enhanced and was moderately less at high pH. This can be attributed to the fact that at lower pH, the surface of photocatalyst is more positively charged, and EY is an anionic dye that favours the efficient adsorption on photocatalyst. Optimum degradation of EY dye is obtained at pH 4 where in 94.4 % degradation was achieved in 80 min under visible light irradiation. Effect of pH on % adsorption and % conversion of dye in the presence of 30 mg TAZnPc-PANI@Fe_2O_3 on MB and EY are presented in the Fig. 7a and 7b respectively.

4.5.3. Reusability of the catalyst

From the perspective of environmental application recyclability and reusability of photocatalysts is very important. In order to examine the stability and durability of the TAZnPc-PANI@Fe_2O_3 photocatalyst, recycling experiments were performed for the photo-degradation of MB. In reusability studies, spent photocatalyst was recovered by ultracentrifugation, thoroughly washed with double distilled water followed by ethanol, finally dried in oven at 60 °C for 5 h and reused. Under the optimized conditions, the photo degradation experiments were carried out for five successive cycles for MB and results are presented in Fig. 8. The studies showed that the photocatalytic activity of the catalysts remained almost stable with slight reduction in photocatalytic activity in fifth run. The results indicate that TAZnPc-PANI@Fe_2O_3 hybrid catalyst has an excellent stability and can be used for several times without any change in its photocatalytic activity. The FTIR spectra of TAZnPc-PANI@Fe_2O_3 before and after five successive cycles for MB photo degradation is presented in the Fig. S5.

5. Conclusion

In this study TAZnPc-PANI@Fe_2O_3 heteroarchitecture was successful synthesized by in situ oxidative polymerization via simple and effective mechanochemical route under solvent-free condition in agate mortar and pestle by mixing the reactants for 20 minutes. This green synthetic strategy does not involve usage of any acidic medium and solvent hence risks associated with solvent use are eliminated. TAZnPc-PANI@ Fe_2O_3 heteroarchitecture showed excellent photodegradation capability as compared to pristine Fe_2O_3 nanomaterials demonstrating the synergetic effect of TAZnPc-PANI sensitizing Fe_2O_3 under the influence of low power white LED as visible light source. Photodegradation experimental results revealed admirable degradation capability of TAZnPc-PANI@ Fe_2O_3 towards both cationic MB and anionic EY dyes. Even after multiple re-uses the TAZnPc-PANI@Fe_2O_3 heteroarchitecture manifested excellent photocatalytic property with a good stability. Hence, TAZnPc-PANI@ Fe_2O_3 can be considered as a potential alternative to remove toxic organic pollutants from wastewater.

Authorship statement

All persons who meet authorship criteria are listed as authors, and all authors certify that they have participated sufficiently in the work to take public responsibility for the content, including participation in the concept, design, analysis, writing, or revision of the manuscript. Furthermore, each author certifies that this material or similar material has not been and will not be submitted to or published in any other publication before its appearance in the Hong Kong Journal of Occupational Therapy.

Authorship contributions

Please indicate the specific contributions made by each author (list the authors' initials followed by their surnames, e.g., Y.L. Cheung). The name of each author must appear at least once in each of the three categories below.

Category 1

Conception and design of study: S. Rajappa, M. C. Devendrachari and H. M. N. Kotresh; acquisition of data: S. Rajappa, P. G. Shivarathri, A. K. M. Laxmipathi, D. K. Swamygowda; analysis and/or interpretation of data: S. Rajappa, M. C. Devendrachari and H. M. N. Kotresh.

Category 2

Drafting the manuscript: S. Rajappa, M. C. Devendrachari and H. M. N. Kotresh; revising the manuscript critically for important intellectual content: M. C. Devendrachari and H. M. N. Kotresh.

Category 3

Approval of the version of the manuscript to be published (the names of all authors must be listed):

S. Rajappa, P. G. Shivarathri, A. K. M. Laxmipathi, D. K. Swamygowda, M. C. Devendrachari, H. M. N. Kotresh.

Declaration of Competing Interest

The authors declare that they have no known competing financial interests or personal relationships that could have appeared to influence the work reported in this paper.

Acknowledgements

All persons who have made substantial contributions to the work reported in the manuscript (e.g., technical help, writing and editing assistance, general support), but who do not meet the criteria for authorship, are named in the Acknowledgements and have given us their written permission to be named. If we have not included an Acknowledgements, then that indicates that we have not received substantial contributions from non-authors.

Supplementary materials

Supplementary material associated with this article can be found, in the online version, at doi:10.1016/j.surfin.2022.101720.

References

[1] Y. Wada, M. Florke, N. Hanasaki, S. Eisner, G. Fischer, S. Tramberend, Y. Satoh, M. T.H. van Vliet, P. Yillia, C. Ringler, P. Burek, D. Wiberg, Geoscientific Model Development 9 (2016) 175–222.
[2] T.I.E. Veldkamp, Y. Wada, J.C.J.H. Aerts, P. Doll, S.N. Gosling, J. Liu, Y. Masaki, T. Oki, S. Ostberg, Y. Pokhre, Y. Satoh, H. Kim, P.J. Ward, Nature Communications 8 (2017) 15697.
[3] C.R. Holkar, A.J. Jadhav, D.V. Pinjari, N.M. Mahamuni, A.B. Pandit, Journal of Environmental Management 182 (2016) 351–366.
[4] T. Deblonde, Carole Cossu-Leguille, Philippe Hartemann, International Journal of Hygiene and Environmental Health 214 (2011) 442–448.
[5] B. Lellis, C.Z. Favaro-Polonio, J.A. Pamphile, J.C. Polonio, Biotechnology Research and Innovation 3 (2019) 275–290.
[6] A. Tkaczyk, K. Mitrowska, A. Posyniak, Science of the Total Environment 717 (2020), 137222.
[7] R. Gusain, K. Gupta, P. Joshi, O.P. Khatri, Advances in Colloid and Interface Science 272 (2019), 102009.
[8] K.Kaur Parul, P.P.Singh R.Badru, S.Kaushal P, Journal of Environmental Chemical Engineering 8 (2020), 103666.
[9] V.S. Kirankumar, S. Sumathi, Materials Today Chemistry 18 (2020), 100355.
[10] D. Chen, Y. Cheng, N. Zhou, P. Chen, Y. Wang, K. Li, S. Huo, P. Cheng, P. Peng, R. Zhang, L. Wang, H. Liu, Y. Liu, R. Ruan, Journal of Cleaner Production 268 (2020), 121725.
[11] P. Singh, A. Borthakur, Journal of Cleaner Production 196 (2018) 1669–1680.
[12] N. Singh, J. Prakash, R.K. Gupta, Molecular Systems Design & Engineering 2 (2017) 422–439.
[13] P. Riente, T. Noel, Catalysis Science & Technology 9 (2019) 5186–5232.
[14] H. Chen, L. Wang, Beilstein Journal of Nanotechnology 5 (2014) 696–710.
[15] S.H. Wu, J.L. Wu, S.Y. Jia, Q.W. Chang, H.T. Ren, Y. Liu, Applied Surface Science 287 (2013) 389–396.
[16] L. Fernandez, V.I. Esteves, A. Cunha, R.J. Schneider, J.P. Tome, Journal of Porphyrins and Phthalocyanines 20 (2016) 150–166.
[17] G.M. Neelgund, A. Oki, Z. Luo, Journal of Colloid and Interface Science 430 (2014) 257–264.
[18] D.K. Kumar, J. Kriz, N. Bennett, B. Chen, H. Upadhayaya, K.R. Reddy, V. Sadhu, Materials Science for Energy Technologies 3 (2020) 472–481.
[19] M.C. Devendrachari, C. Basappa, R. Thimmappa, Z.M. Bhat, M.N.K. Harish, A. R. Kottaichamy, S. Varhade, S. Khaire, K.R.V. Reddy, M.O. Thotiyl, ChemElectroChem 5 (2018) 1817–1821.
[20] M.C. Devendrachari, R. Thimmappa, Z.M. Bhat, S.P. Shafi, M.N.K. Harish, A. R. Kottaichamy, K.R.V. Reddy, M.O. Thotiyl, Sustainable Energy Fuels 2 (2018) 1813–1819.
[21] A.R. Kottaichamy, M.N.K. Harish, M.C. Devendrachari, R. Thimmappa, B. Paswan, O. Tiwari, V. Chanda, P. Gaikwad, M.O. Thotiyl, The Journal of Physical Chemistry C 119 (2015) 28276–28284.
[22] A.R. Kottaichamy, S. Begum, M.C. Devendrachari, Z.M. Bhat, R. Thimmappa, M.N. K. Harish, C.P. Vinod, M.O. Thotiyl, Analytical Chemistry 92 (2020) 4541–4547.
[23] S.M. Sudhakara, M.C. Devendrachari, M.N.K. Harish, F. Khan, Microchemical Journal 161 (2021), 105781.
[24] S.M. Sudhakara, M.C. Devendrachari, M.N.K. Harish, F. Khan, Journal of Electroanalytical Chemistry 884 (2021), 115071.
[25] S.M. Sudhakara, M.C. Devendrachari, M.N.K. Harish, F. Khan, Electroanalysis 32 (8) (2020) 1807–1817.
[26] Y. Zhang, Z. Chen, J. Li, Z Lu, X. Wang, Journal of Energy Chemistry 54 (2021) 36–44.
[27] Q. Dong, Z. Chen, B. Zhao, Y. Zhang, Z. Lu, X. Wang, J. Li, W. Chen, Journal of Colloid and Interface Science 608 (2022) 1951–1959.
[28] M.N.K. Harish, J. Keshavayya, K.R.V. Reddy, H.R. Mallikarjuna, R.A.S. Ali, T. Rajesh, Journal of Coordination Chemistry 63 (2010) 4050–4060.
[29] M.N.K. Harish, J. Keshavayya, K.R.V. Reddy, H.R. Mallikarjuna, Journal of Coordination Chemistry 64 (2011) 2075–2087.
[30] X. Li, K. Kawai, M. Fujitsuka, Y. Osakada, Surfaces and Interfaces 25 (2021), 101249.
[31] Y. Zhang, J.F. Lovell, Wiley Interdisciplinary Reviews: Nanomedicine and Nanobiotechnology 9 (2017) 1420.
[32] N.T. Boileau, O.A. Melville, B. Mirka, R. Cranston, B.H. Lessard, RSC Advances 9 (2019) 2133–2142.
[33] S. Wei, H. Zou, W.Rong H, F. Zhang, Y. Ji, L. Duan, Applied Catalysis B: Environmental 284 (2020), 119739.
[34] H.H. Mohamed, I. Hammami, S. Akhtar, T.E. Youssef, Composites Part B: Engineering 176 (2019), 107314.
[35] J. Tong, D. Wang, F.Xu D.Wang, R. Duan, D. Zhang, J. Fan, B. Dong, Langmuir 36 (2019) 6930–6937.
[36] G.B. Dindaş, Z. Şahin, H.Y. Cengiz, U. Isci, Journal of Porphyrins and Phthalocyanines 23 (2019) 561–568.
[37] T.T. Feng, H. Yin, H. Jiang, X. Chai, X. Li, D. Li, J. Wu, X. Liu, B. Sun, New Journal of Chemistry 43 (2019) 9606.
[38] W. Dai, L. Jiang, J. Wang, Y. Pu, Y. Zhu, Y. Wang, B. Xiao, Chemical Engineering Journal 397 (2019), 125476.
[39] K. Yao, Y. Liu, H. Yang, J. Yuan, S. Shan, Colloids and Surfaces A: Physicochemical and Engineering Aspects 603 (2020), 125240.
[40] M. Samanta, M. Mukherjee, U.K. Ghorai, C. Bose, K.K. Chattopadhyay, Materials Research Bulletin 123 (2020), 110725.
[41] V. Purcar, V. Raditoiu, A. Raditoiu, F.M. Raduly, R. Manea, A. Frone, M. Anastasescu, G.C. Ispas, S. Caprarescu, Materials Research Bulletin 138 (2021), 111222.
[42] K.D. Harris, Nature Chemistry 5 (2013) 12–14.
[43] R.T. O'Neill, R. Boulatov, Nature Reviews Chemistry 5 (2021) 148–167.
[44] J.L. Do, T. Friscic, ACS Central Science 3 (2017) 13–19.
[45] D. Tan, F. Garcia, Chemical Society Reviews 48 (2019) 2274–2292.
[46] P. Ying, J. Yu, W. Su, Advanced Synthesis & Catalysis 363 (2021) 1246–1271.
[47] J. Andersen, J. Mack, Green Chemistry 20 (2018) 1435–1443.
[48] T. Friscic, C. Mottillo, H.M. Titi, Angewandte Chemie 132 (2020) 1030–1041.
[49] E. Boldyreva, Chemical Society Reviews 42 (2013) 7719–7738.
[50] M. Leonardi, M. Villacampa, J.C. Menendez, Chemical Science 9 (2018) 2042–2064.
[51] Y. Chen, G. Mellot, D. van Luijk, C. Creton, R.P. Sijbesma, Chemical Society Reviews 50 (2021) 4100–4140.
[52] A.P. Amrute, B. Zibrowius, F. Schüth, Chemistry of Materials 32 (2020) 4699–4706.
[53] D. Chen, J. Zhao, P. Zhang, S. Dai, Polyhedron 162 (2019) 59–64.
[54] T. Stolar, K. Uzarevic, CrystEngComm 22 (2020) 4511–4525.
[55] E.M. Saggioro, A.S. Oliveira, T. Pavesi, C.G. Maia, L.F.V. Ferreira, J.C. Moreira, Molecules 16 (2011) 10370–10386.
[56] R. Kralchevska, M. Milanova, M. Bistan, A. Pintar, D. Todorovsky, Reaction Kinetics, Mechanisms and Catalysis 109 (2013) 355–373.
[57] M.S.A. Wahab, A. Jilani, I.S. Yahia, A.A. Al-Ghamdi, Superlattices and Microstructures 94 (2016) 108–118.
[58] S. Xun, Z. Zhang, T. Wang, D. Jiang, H. Li, Journal of Alloys and Compounds 685 (2016) 647–655.
[59] W.K. Jo, R.J. Tayade, Industrial & Engineering Chemistry Research 53 (2014) 2073–2084.
[60] Y. Liu, J. Liu, Y. Lin, Y. Zhang, Y. Wei, Ceramics International 35 (2009) 3061–3065.
[61] M. Nafradi, K. Hernadi, Z. Konya, T. Alapi, Chemosphere 280 (2021), 130636.
[62] X. Wei, C.C Wang, Y. Li, P. Wang, Q. Wei, Chemosphere 280 (2021), 130734.
[63] X. Wei, P. Wang, H. Fu, C. Zhao, C.C. Wang, Materials Research Bulletin 129 (2020), 110903.
[64] Y.X. Li, X. Wang, C.C. Wang, H. Fu, Y. Liu, P. Wang, C. Zhao, Journal of Hazardous Materials 399 (2020), 123085.
[65] W.K. Jo, R.J. Tayade, Chinese Journal of Catalysis 35 (2014) 1781–1792.
[66] L.G. Devi, R. Shyamala, Materials Chemistry Frontiers 2 (2018) 796–806.
[67] S. Nag, A. Roychowdhury, D. Das, S. Mukherjee, Materials Research Bulletin 74 (2016) 109–116.
[68] E. Jiang, C. He, X. Xiao, Y. Dong, Y. Gao, Z. Chen, Y. Wu, W. Song, Optical Materials 64 (2017) 193–202.
[69] M. Samanta, U.K. Ghorai, B. Das, P. Howli, S. Das, D. Sen, K.K. Chattopadhyay, RSC Advances 6 (2016) 42739–42744.
[70] M.M. El-nahass, H.M. Zeyada, Optical Materials 27 (2004) 491–498.
[71] D.M. Mafukidze, T. Nyokong, Journal of Coordination Chemistry 8972 (2017) 3598–3618.
[72] O. Nanoparticles, L.E. Mathevula, L.L. Noto, B.M. Mothudi, M.S. Dhlamini, Journal of Luminescence 192 (2017) 879–887.
[73] X. Liu, S. Fu, H. Xiao, C. Huang, Journal of Solid State Chemistry 178 (2005) 2798–2803.
[74] P. Shikha, B.S. Randhawa, T.S. Kang, RSC Advances 5 (2015) 51158–51168.